Keldysh Institute • Publication search

Keldysh Institute preprints • Preprint No. 7, 2015

Kokonkov N.I., Nikolaeva O.V.

Consistent P_1 Synthetic Acceleration of Inner Transport Iterations in 3D Geometry

Recommended form of bibliographic references: Kokonkov N.I., Nikolaeva O.V. Consistent P_1 Synthetic Acceleration of Inner Transport Iterations in 3D Geometry // Keldysh Institute Preprints. 2015. No. 7. 28 p. URL: **http://library.keldysh.ru/preprint.asp?id=2015-7&lg=e**

Keldysh Institute of Applied Mathematics
(Russian Academy of Sciences)

N. I. Kokonkov, O. V. Nikolaeva

Consistent P_1 Synthetic Acceleration of Inner Transport Iterations in 3D Geometry

Moscow — 2015

Kokonkov Nikita Igorevich, Nikolaeva Olga Vasilievna

Consistent P_1 Synthetic Acceleration of Inner Transport Iterations in 3D Geometry

For the KP_1 iterative transport method the production procedure of its "P_1" step consistent with an arbitrary spatial approximation of the S_N transport equation in 3D Cartesian geometry is presented. The procedure is applied to the nodal schemes approximating the within-group S_N transport equation on the unstructured tetrahedral mesh. Produced P_1 synthetic accelerations are experimentally shown to be numerically effective on several model problems.

Keywords: *transport iterations acceleration, KP_1 method, DSA method, nodal scheme, 3D unstructured mesh*

Коконков Никита Игоревич, Николаева Ольга Васильевна

Согласованное P_1 синтетическое ускорение внутренних итераций при решении уравнения переноса в трёхмерной геометрии

Для итерационного KP_1 метода решения уравнения переноса представлена процедура получения "P_1" шага, согласованного с любой пространственной аппроксимацией угловой S_N аппроксимации уравнения переноса в трёхмерной декартовой геометрии. Процедура применена к нодальным сеточным схемам аппроксимации внутригруппового S_N уравнения переноса на неструктурированных тетраэдрических сетках. Вычислительная эффективность полученного P_1 синтетического ускорения показана в численных экспериментах с модельными задачами.

Ключевые слова: *уравнение переноса, ускорение простых итераций метода источника, KP_1 метод, DSA метод, нодальные схемы, неструктурированные трёхмерные сетки*

Table of Contents

Introduction

In the computation particle transport the accurate simulation of the particle interactions with matter is the most challenging problem. Such processes are usually described by a transport equation [1]. To conduct numerical experiments with the system described by the transport equations the last should be discretized into a system of algebraic equations and the resulting system should be numerically solved. The numerical solving of the system is performed by iterative methods.

In the early 1960's were developed the first acceleration methods of the source iteration scheme for S_N problems [2], i.e. transport problems with the S_N (discrete-ordinates) angular approximation. Nowadays the most popular acceleration methods are Goldin's quasi-diffusion method [3-6], Germogenova's average fluxes method [7, 8], and preconditioning methods – Lebedev KP method [9, 10] and introduced by Kopp synthetic method [11-20]. Comprehensive information on development of the source iteration acceleration techniques could be found in the survey [2] by Adams and Larsen.

The preconditioning methods were explored independently by Lebedev [9] and Kopp [11] in the early 1960's and became one of the main paths that researchers have taken. For the diamond-differenced schemes Alcouffe showed [12] that consistent with the S_N transport operator discretization of auxiliary acceleration equations is rapidly convergent for all spatial mesh thicknesses. In one-dimension planar geometry Morel showed [13] that accelerating both the scalar and vector fluxes using the solution of the low-order diffusion synthetic method calculations remedies degraded performance of DSA applied to problems with highly anisotropic scattering. Larsen generalized [14-16] Alcouffe's ideas and developed a procedure to produce consistent low-order equations of the synthetic method for the every standard spatially differenced S_N transport equations. Khalil applied [17] DSA method to accelerate the nodal S_N calculations. Turcksin and Ragusa applied [18] it to the bilinear discontinuous finite element method. Suslov [19], and also Le Tellier and Hébert [20] modified DSA method for the characteristics method transport calculations acceleration. Voloshchenko modified [10] Larsen "four step" procedure [16] and applied it to produce low-order equations consistent with the weighted diamond difference scheme of the "P_1" step of the KP_1 method.

This work is devoted to generalization of that approach to arbitrary spatial discretization of the S_N transport equations and production of the synthetic P_1 equations consistent with the nodal schemes on the tetrahedral mesh for the transport equation [21]. The derived equations are linear system that may be solved by the Krylov subspace methods [22-24]. That acceleration of nodal S_N calculations is tested on the model problems [17, 25, 26].

Base problem formulated in the first section. In the second section P_1 equations in the additive correction produced regardless of the spatial discretization. Nodal spatial approximation applied to the produced equations in the third section. In the forth section acceleration algorithm is described. Model test problems and results of

numerical experiments with them are listed in the fifth and sixth sections. Summary of the results and conclusions are in the seventh section.

Transport equation

Base equations for computations is the multigroup approximation of the time-independent transport equation in the convex region V

$$\begin{aligned}\boldsymbol{\Omega}\cdot\nabla\psi_g(\boldsymbol{\Omega},\mathbf{r})+\sigma^g(\mathbf{r})\psi_g(\boldsymbol{\Omega},\mathbf{r})=\int\limits_{4\pi}\sigma_{gg}(\boldsymbol{\Omega}\cdot\boldsymbol{\Omega}',\mathbf{r})\psi_g(\boldsymbol{\Omega}',\mathbf{r})d\boldsymbol{\Omega}'+\\ +q_g(\mathbf{r})+\sum_{g'\neq g}\int\limits_{4\pi}\nu^{g'}\sigma_{g'g}(\boldsymbol{\Omega}\cdot\boldsymbol{\Omega}',\mathbf{r})\psi_{g'}(\boldsymbol{\Omega}',\mathbf{r})d\boldsymbol{\Omega}'+\\ +\sum_{g'}\int\limits_{4\pi}\nu^{g'f}\sigma_{g'fg}(\boldsymbol{\Omega}\cdot\boldsymbol{\Omega}',\mathbf{r})\psi_{g'}(\boldsymbol{\Omega}',\mathbf{r})d\boldsymbol{\Omega}'\end{aligned} \quad (1)$$

with the boundary conditions

$$\psi_g\left(\boldsymbol{\Omega},\mathbf{r}\big|_{\partial V}\right)=\psi^g_{\partial V}\left(\boldsymbol{\Omega},\mathbf{r}\big|_{\partial V}\right),\quad \mathbf{n}_{\mathbf{r}\partial V}\cdot\boldsymbol{\Omega}<0. \quad (2)$$

The symbols in the equations (1) and (2) defined as follows:

ψ_g – the angular flux distribution as a function of the spatial coordinates $\mathbf{r}$, and the angular direction $\boldsymbol{\Omega}$ for the group g;

σ^g – the macroscopic total cross-section for the group g;

$\sigma_{g'g}$ – the macroscopic differential (elastic) scattering cross-section from the group g' and the angular direction $\boldsymbol{\Omega}'$ to the group g and the angular direction $\boldsymbol{\Omega}$;

$\sigma_{g'fg}$ – the macroscopic differential fission cross-section from the group g' and the angular direction $\boldsymbol{\Omega}'$ to the group g and the angular direction $\boldsymbol{\Omega}$;

$\nu^{g'}$ – the mean number of particles produced due to scattering in the group g';

$\nu^{g'f}$ – the mean number of particles produced due to fission in the group g';

q_g – the spatial extraneous source distribution in the group g;

$\mathbf{n}_{\mathbf{r}\partial V}$ – the outward directed normal of a boundary surface ∂V of the convex region V in boundary point with the spatial coordinates $\mathbf{r}\big|_{\partial V}$;

$\psi^g_{\partial V}$ – the angular flux distribution at boundary surface as function of the inward angular direction $\boldsymbol{\Omega}$ for the group g.

In the Cartesian system an angular direction is specified by a unit vector $\boldsymbol{\Omega}$ that may be defined by the azimuth φ and polar θ angles as demonstrated in the *Figure 1* with the coordinates

$$\Omega_x=\sin\theta\cos\varphi,\quad \Omega_y=\sin\theta\sin\varphi,\quad \Omega_z=\cos\theta. \quad (3)$$

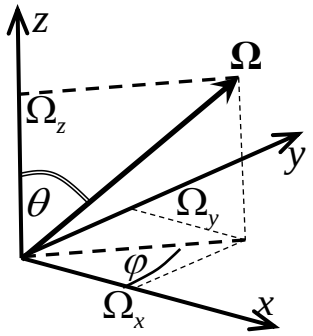

Figure 1
Angular direction
and its coordinates

The transport equation (1) with the boundary conditions (2) must, as a practical matter, be numerically solved iteratively. The standard approach to the iterative solving is splitting iterative process in the two kinds of iteration circles: inner and outer. The inner iterations circle is the sequence of the within-group transport iterations. The ι^{th} step of the inner iterations started with distribution of zero describes a single group particles that undergone ι collisions. The outer iterations are a wider circle of the inter-group scattering and fission, including inner iterations as a sub-circle. The υ^{th} step of the outer iterations describes the multigroup particles distributions that undergone υ interaction events resulted in their emission and relocation between energy groups. The urge necessity is the acceleration of the inner iterations process which converges rather slowly for problems where the most of the particles undergo many collisions.

P_1 consistent acceleration

The first synthetic acceleration equations in additive correction originate from the physical grasp of the scattering occurrence in both sides of the transport equations. And to eliminate effect of the scattering source integral of the previous source iteration solution in right hand side the left hand side scattering hidden in the total adsorption may be used. The next idea is reducing order of such equations. It may be performed in two ways: reduction of the number of spatial elements for discretization and angular order lowering. The second approach is more obvious one to get auxiliary low-order accelerating equation consistent with the spatial approximation of the base transport equation. Following the Voloshchenko modification [10] of the Larsen "four step" procedure [16] low-order P_1 synthetic equations in additive correction consistent with the arbitrary spatial discretization will be produced.

I Omitting for convenience the group indices for the inner transport iterations the within-group transport equation may be written in the operator form

$$\hat{L}\psi = \hat{S}\psi + q, \qquad (4)$$

where the leakage and collision operator is

$$\hat{L} = \mathbf{\Omega} \cdot \nabla + \sigma_t; \tag{5}$$

the scattering source operator applied to an arbitrary angular function ϕ is

$$\hat{S}\phi = \int_{4\pi} \sigma(\mathbf{\Omega} \cdot \mathbf{\Omega}')\phi(\mathbf{\Omega}')d\mathbf{\Omega}'; \tag{6}$$

ψ – the within-group flux distribution as a function of the spatial coordinates $\mathbf{r}$, and the angular direction $\mathbf{\Omega}$ resulted from the exact solution of the transport equation;

σ_t – the within-group macroscopic total cross-section;

σ – the within-group macroscopic differential scattering from the angular direction $\mathbf{\Omega}$ to the angular direction $\mathbf{\Omega}'$ cross-section;

q – the within-group spatial extraneous source distribution with the source from the outer iterations.

II Derived from the exact equation (4) the source iterations equation in the operator form is

$$\hat{L}\overset{1/2}{\psi} = \hat{S}\overset{0}{\psi} + q \tag{7}$$

where the actual inner iteration index $\imath$ is suppressed and

$\overset{1/2}{\psi}$ – the within-group angular flux distribution as a function of the spatial coordinates $\mathbf{r}$, and the angular direction $\mathbf{\Omega}$ resulted from a single transport sweep;

$\overset{0}{\psi}$ – the within-group angular flux distribution as a function of the spatial coordinates $\mathbf{r}$, and the angular direction $\mathbf{\Omega}$ resulted from previous inner iteration.

III By subtracting the equation (7) from the equation (4)

$$\hat{L}\left(\psi - \overset{1/2}{\psi}\right) = \hat{S}\left(\left(\psi - \overset{1/2}{\psi}\right) + \left(\overset{1/2}{\psi} - \overset{0}{\psi}\right)\right) \tag{8}$$

the exact equation for the exact additive correction $\overset{1/2}{f} = \psi - \overset{1/2}{\psi}$ is obtained

$$\hat{L}\overset{1/2}{f} = \hat{S}\overset{1/2}{f} + \hat{S}\left(\overset{1/2}{\psi} - \overset{0}{\psi}\right) \tag{9}$$

from which the exact solution of the within-group transport equation (4) could be obtained in two steps with a single transport sweep (7) as the first step. The idea of P_1 synthetic acceleration is to replace the equation (9) by low order equations with low order approximations of the additive correction and the $L - S$ operator.

IV By linear in solid angle approximation of the additive correction

$$\overset{1/2}{f} = U + \mathbf{\Omega}\cdot\boldsymbol{W}, \tag{10}$$

where the U and $\boldsymbol{W}$ are the approximation quotients, the equation (9) may be written

$$\hat{L}U + \hat{L}\left(\mathbf{\Omega}\cdot\boldsymbol{W}\right) = \hat{S}\left(U + \mathbf{\Omega}\cdot\boldsymbol{W}\right) + \hat{S}\varepsilon \tag{11}$$

where the flux increment $\varepsilon = \overset{1/2}{\psi} - \overset{0}{\psi}$.

In the equation (11) in the U and $\boldsymbol{W}$ the within-group scattering partly eliminated. As it would be desirable for convergence improvement.

V The last procedure step is the equation (11) order lowering by its integrations with weights 1 and $\mathbf{\Omega}$ over solid angle. That would obviously lead to the diffusion type equation system which coefficients and unknowns do not depend on the angular direction. In practice that integrations could be performed only numerically for an angular discretization of the (11). The most straightforward way of the angular discretization is the discrete directions set usage instead of the continuous one.

The S_N method [1] also referred as the discrete-ordinates method essential basis is that the flux angular distribution is evaluated in the number of discrete directions. This enables usage of various quadrature sets in the angular directions domain to numerically calculate scattering integrals. The angular quadrature set are specified by the set of angular directions $\{\mathbf{\Omega}_d\}$ and the corresponding set of quadrature weights $\{w_d\}$ such that the integrals over solid angle may be suitably approximated by summation over the quadrature set

$$\int_{4\pi} \phi\left(\mathbf{\Omega}\right) d\mathbf{\Omega} \approx \sum_d w_d \phi\left(\mathbf{\Omega}_d\right). \tag{12}$$

The equations (4)-(10) may be rewritten in the S_N form. Thus the S_N discretization of the equation (11) may be derived, and the final step V may be accomplished by the numerical integration.

I For an arbitrary angular quadrature set the S_N approximation of the exact transport equation (4) along the angular direction $\mathbf{\Omega}_d$ from the set is

$$\hat{L}_d \psi_d = \hat{S}_d \psi + q_d, \tag{13}$$

the leakage and collision operator (5) along the angular direction $\mathbf{\Omega}_d$ is

$$\hat{L}_d = \mathbf{\Omega}_d \cdot \nabla + \sigma_t; \tag{14}$$

the scattering source operator (6) along the angular direction $\mathbf{\Omega}_d$ applied to an arbitrary angular function ϕ is

$$\hat{S}_d\phi = \int_{4\pi} \sigma\left(\boldsymbol{\Omega}_d \cdot \boldsymbol{\Omega}'\right)\phi\left(\boldsymbol{\Omega}'\right)d\boldsymbol{\Omega}'; \tag{15}$$

ψ_d – the within-group flux distribution along the angular direction $\boldsymbol{\Omega}_d$ as a function of the spatial coordinates $\mathbf{r}$;
q_d – the within-group spatial extraneous source distribution with the source from the outer iterations along the angular direction $\boldsymbol{\Omega}_d$.

II The S_N approximation of the source iterations equation (7) is

$$\hat{L}_d \overset{1/2}{\psi}_d = \hat{S}_d \overset{0}{\psi} + q_d \tag{16}$$

$\overset{1/2}{\psi}_d$ – the within-group flux distribution along the angular direction $\boldsymbol{\Omega}_d$ as a function of the spatial coordinates $\mathbf{r}$ resulted from a single transport sweep.

III For the additive correction $\overset{1/2}{f}_d = \psi_d - \overset{1/2}{\psi}_d$ along the angular direction $\boldsymbol{\Omega}_d$ the S_N approximation of the equation (9) is

$$\hat{L}_d \overset{1/2}{f}_d = \hat{S}_d \overset{1/2}{f} + \hat{S}_d\left(\overset{1/2}{\psi} - \overset{0}{\psi}\right) \tag{17}$$

IV By the linear in solid angle approximation of the additive correction along the angular direction $\boldsymbol{\Omega}_d$

$$\overset{1/2}{f}_d = U + \boldsymbol{\Omega}_d \cdot \boldsymbol{W} \tag{18}$$

the equation (17) may be written

$$\hat{L}_d U + \hat{L}_d\left(\boldsymbol{\Omega}_d \cdot \boldsymbol{W}\right) = \hat{S}_d\left(U + \boldsymbol{\Omega} \cdot \boldsymbol{W}\right) + \hat{S}_d\varepsilon \tag{19}$$

The macroscopic differential scattering cross-section from the angular direction $\boldsymbol{\Omega}'$ to the angular direction $\boldsymbol{\Omega}_d$ may be expanded in Legendre polynomial series

$$\sigma\left(\boldsymbol{\Omega}_d \cdot \boldsymbol{\Omega}'\right) = \frac{\sigma_0}{4\pi} + \frac{3\sigma_1}{4\pi}\boldsymbol{\Omega}_d \cdot \boldsymbol{\Omega}' + \ldots \tag{20}$$

with the expansion quotients σ_0, σ_1, and so forth. Hence due to orthogonality of the Legendre polynomials the scattering source operator (15) with the scattering cross-section (20) applying to the additive correction (10) leads to

$$\hat{S}_d\left(U + \boldsymbol{\Omega} \cdot \boldsymbol{W}\right) = \sigma_0 U + \sigma_1 \boldsymbol{\Omega}_d \cdot \boldsymbol{W}. \tag{21}$$

And the equation (19) finally may be written as

$$\hat{L}_d U + \hat{L}_d \left(\mathbf{\Omega}_d \cdot \boldsymbol{W} \right) - \left(\sigma_0 U + \sigma_1 \mathbf{\Omega}_d \cdot \boldsymbol{W} \right) = \hat{S}_d \varepsilon . \tag{22}$$

V Summation of the equation (22) over the given angular quadrature set with the integration weight 1 leads to equation

$$\begin{gathered} \sum_d w_d L_d U - \sigma_0 \left(\sum_d w_d \right) U + \\ + \sum_\beta \sum_d w_d \Omega_{d\beta} L_d W_\beta - \sigma_1 \sum_\beta \left(\sum_d w_d \Omega_{d\beta} \right) W_\beta = \sum_d w_d \hat{S}_d \varepsilon \end{gathered} \tag{23}$$

and summation of the equation (22) over the given angular quadrature set with the integration weight Ω_γ leads to vector equation

$$\begin{gathered} \sum_d w_d \Omega_{d\gamma} L_d U - \sigma_0 \left(\sum_d w_d \Omega_{d\gamma} \right) U + \\ + \sum_\beta \sum_d w_d \Omega_{d\gamma} \Omega_{d\beta} L_d W_\beta - \sigma_1 \sum_\beta \left(\sum_d w_d \Omega_{d\gamma} \Omega_{d\beta} \right) W_\beta = \sum_d w_d \Omega_{d\gamma} \hat{S}_d \varepsilon \end{gathered} \tag{24}$$

where β and γ run over x, y, and z.

Thus the production of the P_1 synthetic acceleration equations consistent with an arbitrary spatial approximation has been accomplished in five steps. The equations (23)-(24) in the U and $\boldsymbol{W}$ system, which coefficients and unknowns do not depend on the angular direction, is the low order approximation to the equation (17). Solution of this system gives the low order approximation (10) to the additive correction as the linear function of the angular direction.

Spatial approximation

By repeating the same five step procedure for the equations (13)-(19) with the spatially approximated starting S_N transport equation (13) the consistent spatial approximation of the equations (23)-(24) system may be derived.

To get spatial approximation of the equations (13)-(19) with the nodal schemes [21] an unstructured tetrahedral spatial mesh in the convex region V may be introduced and all spatial functions in the region may be approximated by vectors of the functions values in the spatial mesh cells and faces. The vectors size is a sum of the mesh cells and faces numbers. The S_N approximation of the leakage and collision operator (14) along the angular direction $\mathbf{\Omega}_d$ is then spatially approximated by the two square matrices $\left(\mathbf{1} - \mathbf{T}_d \right)$ and $\mathbf{G}_d$ of the same size as the spatial functions values vectors, where the square matrix $\mathbf{T}_d$ has zero diagonal elements. Thus the spatial

approximation of the S_N angular approximation of the transport equation (13) along the angular direction $\mathbf{\Omega}_d$ is

$$\text{I} \qquad \left(\mathbf{1}-\mathbf{T}_d\right)\boldsymbol{\psi}_d = \mathbf{G}_d\left(\hat{S}_d\boldsymbol{\psi}+\mathbf{q}_d\right), \tag{25}$$

and the source iterations equation (16) spatial approximation is

$$\text{II} \qquad \left(\mathbf{1}-\mathbf{T}_d\right)\overset{1/2}{\boldsymbol{\psi}}_d = \mathbf{G}_d\left(\hat{S}_d\overset{0}{\boldsymbol{\psi}}+\mathbf{q}_d\right). \tag{26}$$

$\boldsymbol{\psi}_d$ – the vector of the values in the spatial mesh cells and faces of the within-group flux distribution along the angular direction $\mathbf{\Omega}_d$;

$\boldsymbol{\psi}$ – the vector of the values in the spatial mesh cells and faces of the within-group angular flux distribution as functions of the angular direction $\mathbf{\Omega}$;

$\mathbf{q}_d$ – the vector of the values in the spatial mesh cells and faces of the within-group spatial extraneous source distribution with the source from the outer iterations along the angular direction $\mathbf{\Omega}_d$;

$\overset{1/2}{\boldsymbol{\psi}}_d$ – the vector of the values in the spatial mesh cells and faces of the within-group flux distribution along the angular direction $\mathbf{\Omega}_d$ resulted from the transport sweep;

$\overset{0}{\boldsymbol{\psi}}$ – the vector of the values in the spatial mesh cells and faces of the within-group angular flux distribution as functions of the angular direction $\mathbf{\Omega}$ resulted from the previous inner iteration step.

The approximated equation (17) in vector of the values in the spatial mesh cells and faces of the additive correction $\overset{1/2}{\mathbf{f}}_d = \boldsymbol{\psi}_d - \overset{1/2}{\boldsymbol{\psi}}_d$ along the angular direction $\mathbf{\Omega}_d$ is

$$\text{III} \qquad \left(\mathbf{1}-\mathbf{T}_d\right)\overset{1/2}{\mathbf{f}}_d = \mathbf{G}_d\hat{S}_d\overset{1/2}{\mathbf{f}} + \mathbf{G}_d\hat{S}_d\left(\overset{1/2}{\boldsymbol{\psi}}-\overset{0}{\boldsymbol{\psi}}\right). \tag{27}$$

With the angular approximation (10) of the additive correction vector

$$\overset{1/2}{\mathbf{f}} = \mathbf{U} + \sum_{\beta}\Omega_{\beta}\mathbf{W}_{\beta}, \tag{28}$$

and the notation (21) of the scattering source operator along the angular direction $\mathbf{\Omega}_d$ the equation (27) may be written

$$\text{IV} \qquad \left(\mathbf{1}-\mathbf{T}_d-\sigma_0\mathbf{G}_d\right)\mathbf{U} + \left(\mathbf{1}-\mathbf{T}_d-\sigma_1\mathbf{G}_d\right)\sum_{\beta}\Omega_{d\beta}\mathbf{W}_{\beta} = \mathbf{G}_d\hat{S}_d\boldsymbol{\varepsilon} \tag{29}$$

where $\mathbf{U}$ and $\mathbf{W}_{\beta}$ are the vectors of the values in the spatial mesh cells and faces of

the additive correction approximation quotients, the flux increment vector $\boldsymbol{\varepsilon} = \overset{1/2}{\boldsymbol{\psi}} - \overset{0}{\boldsymbol{\psi}}$, and β runs over x, y, and z.

Summation of the equation (29) over the given angular quadrature set with the integration weight 1 leads to equation

$$\text{V} \quad \begin{gathered} \sum_d w_d \left(\mathbf{1} - \mathbf{T}_d - \sigma_0 \mathbf{G}_d\right)\mathbf{U} + \\ + \sum_\beta \sum_d w_d \Omega_{d\beta} \left(\mathbf{1} - \mathbf{T}_d - \sigma_1 \mathbf{G}_d\right)\mathbf{W}_\beta = \sum_d w_d \mathbf{G}_d \hat{S}_d \boldsymbol{\varepsilon} \end{gathered} \tag{30}$$

and summation of the equation (29) over the given angular quadrature set with the integration weight Ω_γ leads to vector equation

$$\text{V} \quad \begin{gathered} \sum_d w_d \Omega_{d\gamma} \left(\mathbf{1} - \mathbf{T}_d - \sigma_0 \mathbf{G}_d\right)\mathbf{U} + \\ + \sum_\beta \sum_d w_d \Omega_{d\gamma} \Omega_{d\beta} \left(\mathbf{1} - \mathbf{T}_d - \sigma_1 \mathbf{G}_d\right)\mathbf{W}_\beta = \sum_d w_d \Omega_{d\gamma} \mathbf{G}_d \hat{S}_d \boldsymbol{\varepsilon} \end{gathered} \tag{31}$$

where β and γ run over x, y, and z. The equations (30)-(31) system in the $\mathbf{U}$ and $\mathbf{W}_\beta$ is the low order approximation to the equation (27).

With the notation (20) of the macroscopic differential scattering cross-section the scattering source operator applied to the flux increment vector $\boldsymbol{\varepsilon}$ in the right hand side of the equations (30)-(31) system may be written

$$\hat{S}_d \boldsymbol{\varepsilon} = \frac{\sigma_0}{4\pi} \boldsymbol{\varepsilon}_0 + \frac{3\sigma_1}{4\pi} \sum_\beta \Omega_{d\beta} \boldsymbol{\varepsilon}_\beta \tag{32}$$

where angular moments vectors of the flux increment are

$$\boldsymbol{\varepsilon}_0 = \int_{4\pi} \boldsymbol{\varepsilon}(\boldsymbol{\Omega}) d\boldsymbol{\Omega} \tag{33}$$

and

$$\boldsymbol{\varepsilon}_\beta = \int_{4\pi} \Omega_\beta \boldsymbol{\varepsilon}(\boldsymbol{\Omega}) d\boldsymbol{\Omega} \tag{34}$$

where β runs over x, y, and z.

Boundary conditions should be introduced for the spatial approximation finalization. This may be performed by applying the step V angular summations to the equation (29) with angular dependent coefficients and the same five steps routine to the spatial approximation of the S_N transport boundary condition for inward and outward angular directions respectively.

On boundary mesh face with the outer normal $\mathbf{n}$ summation of the equation (29) over the half where $\mathbf{n}\cdot\mathbf{\Omega}_d > 0$ of the given angular quadrature set with the integration weight 1 leads to

$$\begin{matrix} \sum\limits_{d,\mathbf{n}\cdot\mathbf{\Omega}_d>0} w_d \left(\mathbf{1}-\mathbf{T}_d-\sigma_0\mathbf{G}_d\right)\mathbf{U}+ \\ +\sum\limits_{\beta}\sum\limits_{d,\mathbf{n}\cdot\mathbf{\Omega}_d>0} w_d\Omega_{d\beta}\left(\mathbf{1}-\mathbf{T}_d-\sigma_1\mathbf{G}_d\right)\mathbf{W}_\beta = \sum\limits_{d,\mathbf{n}\cdot\mathbf{\Omega}_d>0} w_d\mathbf{G}_d\hat{S}_d\boldsymbol{\varepsilon} \end{matrix} \quad \text{V} \qquad (35)$$

and summation of the equation (29) over that half of the given angular quadrature set with the integration weight Ω_γ leads to

$$\begin{matrix} \sum\limits_{d,\mathbf{n}\cdot\mathbf{\Omega}_d>0} w_d\Omega_{d\gamma}\left(\mathbf{1}-\mathbf{T}_d-\sigma_0\mathbf{G}_d\right)\mathbf{U}+ \\ +\sum\limits_{\beta}\sum\limits_{d,\mathbf{n}\cdot\mathbf{\Omega}_d>0} w_d\Omega_{d\gamma}\Omega_{d\beta}\left(\mathbf{1}-\mathbf{T}_d-\sigma_1\mathbf{G}_d\right)\mathbf{W}_\beta = \sum\limits_{d,\mathbf{n}\cdot\mathbf{\Omega}_d>0} w_d\Omega_{d\gamma}\mathbf{G}_d\hat{S}_d\boldsymbol{\varepsilon} \end{matrix} \quad \text{V} \qquad (36)$$

where β and γ run over x, y, and z.

Specular reflection boundary condition with the albedo A for the base transport equation (1) in a single group is

$$\psi\left(\mathbf{\Omega}_\partial,\mathbf{r}|_{\partial V}\right) = A\psi\left(\mathbf{\Omega}_d,\mathbf{r}|_{\partial V}\right), \quad \mathbf{\Omega}_\partial = \mathbf{\Omega}_d - 2\left(\mathbf{n}\cdot\mathbf{\Omega}_d\right)\mathbf{n}, \qquad (37)$$

where $\mathbf{\Omega}_\partial$ is the incident ray angular direction and $\mathbf{n}=\mathbf{n}_{\mathbf{r}\partial V}$.

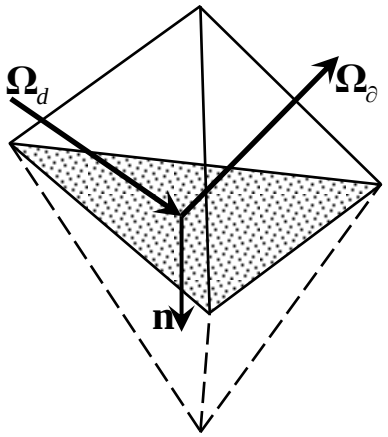

Figure 2

By introducing as on the *Figure 2* the virtual cell that are the mirror reflection of the boundary cell in the boundary face under consideration the specular boundary condition (37) could be introduced in a similar to the equation (25) form. Due to spatial discretization matrices in mirror reflections pairing the exact equation is

$$\left(\mathbf{1}-A\mathbf{T}_d\right)\boldsymbol{\psi}_\partial = A\mathbf{G}_d\left(\hat{S}_\partial\boldsymbol{\psi}+\mathbf{q}_\partial\right), \quad \mathbf{n}\cdot\mathbf{\Omega}_d<0 \quad \text{I} \qquad (38)$$

on the boundary face, the source iterations equation similar to the (26) one is

$$\text{II} \qquad \left(\mathbf{1}-A\mathbf{T}_d\right)\overset{1/2}{\boldsymbol{\psi}}_{\partial}=A\mathbf{G}_d\left(\hat{S}_{\partial}\overset{0}{\boldsymbol{\psi}}+\mathbf{q}_{\partial}\right),\quad \mathbf{n}\cdot\boldsymbol{\Omega}_d<0, \tag{39}$$

and the equation in additive correction similar to the equation (27) is

$$\text{III} \qquad \left(\mathbf{1}-A\mathbf{T}_d\right)\overset{1/2}{\mathbf{f}}_{\partial}=A\mathbf{G}_d\hat{S}_{\partial}\overset{1/2}{\mathbf{f}}+A\mathbf{G}_d\hat{S}_{\partial}\left(\overset{1/2}{\boldsymbol{\psi}}-\overset{0}{\boldsymbol{\psi}}\right),\quad \mathbf{n}\cdot\boldsymbol{\Omega}_d<0, \tag{40}$$

where subscript ∂ stands for the magnitudes along the incident ray $\boldsymbol{\Omega}_{\partial}$.

Introducing the angular approximation (10) and noting the (21) gives

$$\text{IV} \qquad \left(\mathbf{1}-A\mathbf{T}_d-\sigma_0 A\mathbf{G}_d\right)\mathbf{U}+\left(\mathbf{1}-A\mathbf{T}_d-\sigma_1 A\mathbf{G}_d\right)\sum_{\beta}\Omega_{\partial\beta}\mathbf{W}_{\beta}=A\mathbf{G}_d\hat{S}_{\partial}\boldsymbol{\varepsilon}. \tag{41}$$

where β runs over x, y, and z.

Summation of the equation (41) over the half where $\mathbf{n}\cdot\boldsymbol{\Omega}_d<0$ of the given angular quadrature set with the integration weight 1 leads to

$$\text{V} \qquad \begin{gathered}\sum_{d,\mathbf{n}\cdot\boldsymbol{\Omega}_d<0} w_d\left(\mathbf{1}-A\left(\mathbf{T}_d+\sigma_0\mathbf{G}_d\right)\right)\mathbf{U}+\\ +\sum_{\beta}\sum_{d,\mathbf{n}\cdot\boldsymbol{\Omega}_d<0} w_d\Omega_{\partial\beta}\left(\mathbf{1}-A\left(\mathbf{T}_d+\sigma_1\mathbf{G}_d\right)\right)\mathbf{W}_{\beta}=A\sum_{d,\mathbf{n}\cdot\boldsymbol{\Omega}_d<0} w_d\mathbf{G}_d\hat{S}_{\partial}\boldsymbol{\varepsilon}\end{gathered} \tag{42}$$

and summation of the equation (41) over that half of the given angular quadrature set with the integration weight Ω_{γ} leads to

$$\text{V} \qquad \begin{gathered}\sum_{d,\mathbf{n}\cdot\boldsymbol{\Omega}_d<0} w_d\Omega_{\partial\gamma}\left(\mathbf{1}-A\left(\mathbf{T}_d+\sigma_0\mathbf{G}_d\right)\right)\mathbf{U}+\\ +\sum_{\beta}\sum_{d,\mathbf{n}\cdot\boldsymbol{\Omega}_d<0} w_d\Omega_{\partial\gamma}\Omega_{\partial\beta}\left(\mathbf{1}-A\left(\mathbf{T}_d+\sigma_1\mathbf{G}_d\right)\right)\mathbf{W}_{\beta}=A\sum_{d,\mathbf{n}\cdot\boldsymbol{\Omega}_d<0} w_d\Omega_{\partial\gamma}\mathbf{G}_d\hat{S}_{\partial}\boldsymbol{\varepsilon}\end{gathered} \tag{43}$$

where β and γ run over x, y, and z.

Termwise adding the equations (42)-(43) properly to the equations (35)-(36) leads to the equations system in the $\mathbf{U}$ and $\mathbf{W}_{\beta}$. Solution of this system with the equations (30)-(31) system gives the complete low order approximation (28) to the additive correction as the linear function of the angular direction.

The S_N approximation of the spatially approximated non-reflective boundary condition for the transport equation (1) in a single group corresponding to the equation (25)

$$\text{I} \qquad \boldsymbol{\psi}_d^{\partial V}=\mathbf{q}_d^{\partial V},\quad \mathbf{n}\cdot\boldsymbol{\Omega}_d<0, \tag{44}$$

its source iterations form corresponding to the equation (26) is

II
$$\boldsymbol{\psi}_d^{1/2\,\partial V} = \mathbf{q}_d^{\partial V}, \quad \mathbf{n}\cdot\boldsymbol{\Omega}_d < 0, \tag{45}$$

where $\mathbf{n}$ is the boundary face dependent outer normal to that boundary face;
$\boldsymbol{\psi}_d^{\partial V}$ – the vector of the values in the boundary mesh faces of the within-group flux distribution along the angular direction $\boldsymbol{\Omega}_d$;
$\mathbf{q}_d^{\partial V}$ – the vector of the values of the within-group boundary extraneous source distribution along the angular direction $\boldsymbol{\Omega}_d$;
$\boldsymbol{\psi}_d^{1/2\,\partial V}$ – the vector of the values in the boundary mesh faces of the within-group flux distribution along the angular direction $\boldsymbol{\Omega}_d$ resulted from the transport sweep;
sizes of these vectors is an amount of the non-reflective boundary mesh faces.

Subtraction the equation (45) from the equation (44) leads to

$$\mathbf{f}_d^{1/2\,\partial V} = \mathbf{0}, \quad \mathbf{n}\cdot\boldsymbol{\Omega}_d < 0 \tag{46}$$

equation in the additive correction on the boundaries. The equation (46) by introducing the angular approximation (28) on the boundary faces may be written

$$\mathbf{U} + \sum_{\beta} \Omega_\beta \mathbf{W}_\beta = \mathbf{0} \tag{47}$$

where β runs over x, y, and z. Summation of the equation (47) over the half where $\mathbf{n}\cdot\boldsymbol{\Omega}_d < 0$ of the given angular quadrature set with the integration weight 1 leads to

$$\mathbf{U} \sum_{d,\mathbf{n}\cdot\boldsymbol{\Omega}_d<0} w_d + \sum_{\beta} \mathbf{W}_\beta \sum_{d,\mathbf{n}\cdot\boldsymbol{\Omega}_d<0} w_d \Omega_{d\beta} = \mathbf{0} \tag{48}$$

and summation of the equation (47) over that half of the given angular quadrature set with the integration weight Ω_γ leads to

$$\mathbf{U} \sum_{d,\mathbf{n}\cdot\boldsymbol{\Omega}_d<0} w_d \Omega_{d\gamma} + \sum_{\beta} \mathbf{W}_\beta \sum_{d,\mathbf{n}\cdot\boldsymbol{\Omega}_d<0} w_d \Omega_{d\gamma}\Omega_{d\beta} = \mathbf{0} \tag{49}$$

where β and γ run over x, y, and z.

Termwise adding the equations (48)-(49) properly to the equations (35)-(36) leads to the equations system in the $\mathbf{U}$ and $\mathbf{W}_\beta$. Solution of this system with the equations (30)-(31) system gives the complete low order approximation (28) to the additive correction as linear function of angular direction.

Derivation of the consistent synthetic "P_1" step equations of the KP_1 nodal transport calculations on the unstructured tetrahedral mesh is hereby finalized.

Acceleration algorithm

In the iterative KP algorithms the next, $\iota+1$, successive approximation to the exact solution of the within-group transport equation

$$\overset{\iota+1}{\boldsymbol{\psi}}_d = \overset{\iota+1/2}{\boldsymbol{\psi}}_d + \overset{\iota+1/2}{\mathbf{f}}_d \tag{50}$$

is obtained in two steps:

1) "K" step that is a single transport sweep with proper boundary conditions from which the vector $\overset{\iota+1/2}{\boldsymbol{\psi}}_d$ of the values in spatial mesh elements of the within-group flux along the angular direction $\boldsymbol{\Omega}_d$ is obtained,

2) "P" step that is a low order approximation to the equations in the exact additive correction to the within-group source iteration equations solution from which the vector $\overset{\iota+1/2}{\mathbf{f}}_d$ of the values in the spatial mesh elements of the within-group additive correction approximation along the angular direction $\boldsymbol{\Omega}_d$ is obtained.

Applying the KP_1 method with the consistent synthetic "P_1" step to accelerate the nodal S_N transport calculations on the unstructured tetrahedral mesh [21] is reasonably succeeds to the above described two step iterative process. The "K" step is performed in the regular manner of the single source iteration (26) implementation for the given nodal spatial approximation. After it the flux increment vector $\boldsymbol{\varepsilon} = \overset{1/2}{\boldsymbol{\psi}} - \overset{0}{\boldsymbol{\psi}}$ angular moments (33)-(34) are calculated numerically by summations over the given angular quadrature set. And the "P_1" step consists of

a) the spatial approximation matrices along angular directions $\left(\mathbf{1}-\mathbf{T}_d\right)$ and $\mathbf{G}_d$ weighted angular numerical integrations (step V above) which lead to the consistent synthetic P_1 equations system in the coefficients of the additive correction linear approximation,

b) the produced linear equations system solving by the preconditioned generalized minimal residual Krylov method and correction by its solution of the flux values vector obtained in the "K" step.

Corrected flux becomes the next successive approximation to the nodal S_N transport calculations result and used in the next single source iteration of the "K" step. For memory saving purposes the numerical angular integrations of the spatial approximation matrices are performed on the each KP_1 iteration step ι.

In general, the nodal S_N transport calculations result in the polynomial spatial approximations of the fluxes along the given angular directions. In the spatial mesh cells and faces the two nodal schemes under consideration [21] "ThetraC" and "ThetraL" are approximate flux along an angular direction by constant and linear functions respectively. But for further order lowering the derived consistent P_1 synthetic acceleration is used to additively correct only zero spatial moments of the nodal S_N transport calculations results for the both schemes.

Test problems

The effectiveness of the proposed inner iterations acceleration algorithm is tested on the model one group test problems. Their descriptions with materials properties and geometry are listed below.

A The EIR-2a (named after Swiss research facility Eidgenössisches Institut für Reaktorforschung) problem [25] 3D generalization describes particle transport in a uniform prism with vacuum (non-reflective with $\mathbf{q}_d^{\partial V} = \mathbf{0}$) boundary conditions on all its faces consisting of scattering medium **5** with adsorbing inclusions **1**, **2**, **3** and **4**. Materials properties and geometry for this problem are presented in the *Table 1* and the *Figure 3*. The problem is solved on the S_8 [27] angular quadrature set and on the six unstructured tetrahedral spatial meshes sequence with increasing fineness.

Table 1

Materials properties for the EIR-2a problem

Material	**1**	**2**	**3**	**4**	**5**
σ_t (cm^{-1})	0.60	0.48	0.70	0.65	0.90
σ (cm^{-1})	0.53	0.20	0.66	0.50	0.89
Source (cm^{-3})	1.0	0.0	1.0	0.0	0.0

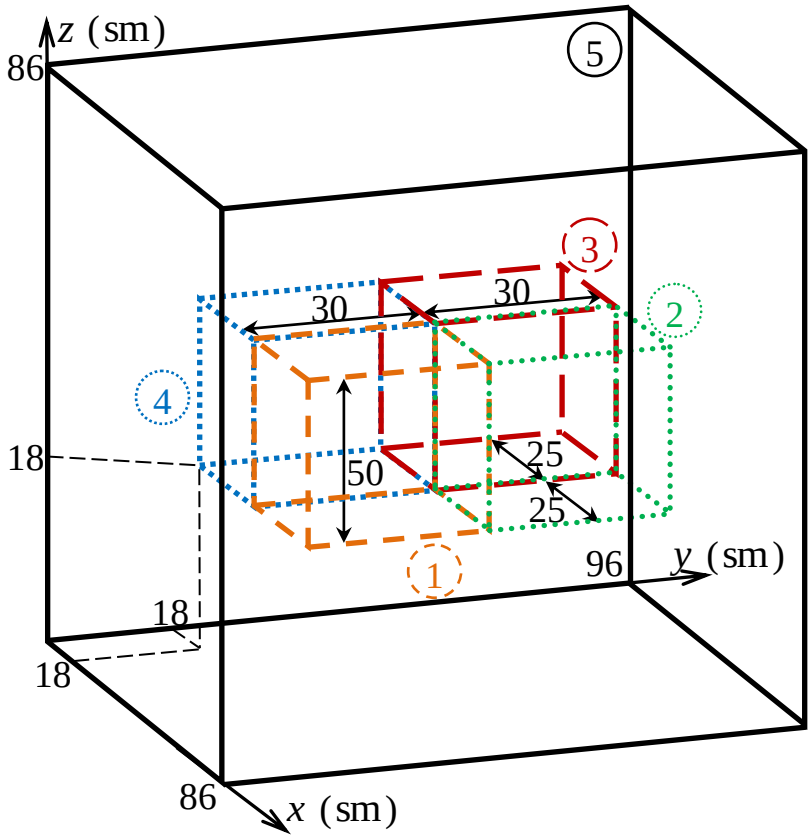

Figure 3

Geometry for the EIR-2a problem

B The Iron-Water problem is the 3D generalization of the model shielding problem [15] 2D generalization [17]. In the problem the neutron transport in PWR is simulated. Materials properties and geometry for this problem are presented in the *Table 2* and the *Figure 4*. Reflective boundary conditions with $A=1$ are used at the boundary planes $x=0$, $y=0$, and $z=0$, and vacuum (non-reflective with $\mathbf{q}_d^{\partial V}=\mathbf{0}$) boundary conditions at all other outer boundaries. The problem is solved on the S_8 [27] angular quadrature set and on the seven unstructured tetrahedral spatial meshes sequence with increasing fineness.

Table 2

Materials properties for the Iron-Water problem

Material	**1**	**2**	**3**
σ_t (cm^{-1})	3.3333	3.3333	1.3333
σ_0 (cm^{-1})	3.3136	3.3136	1.1077
σ_1 (cm^{-1})	0.9256	0.9256	0.9367
Source (cm^{-3})	1.0	0.0	0.0

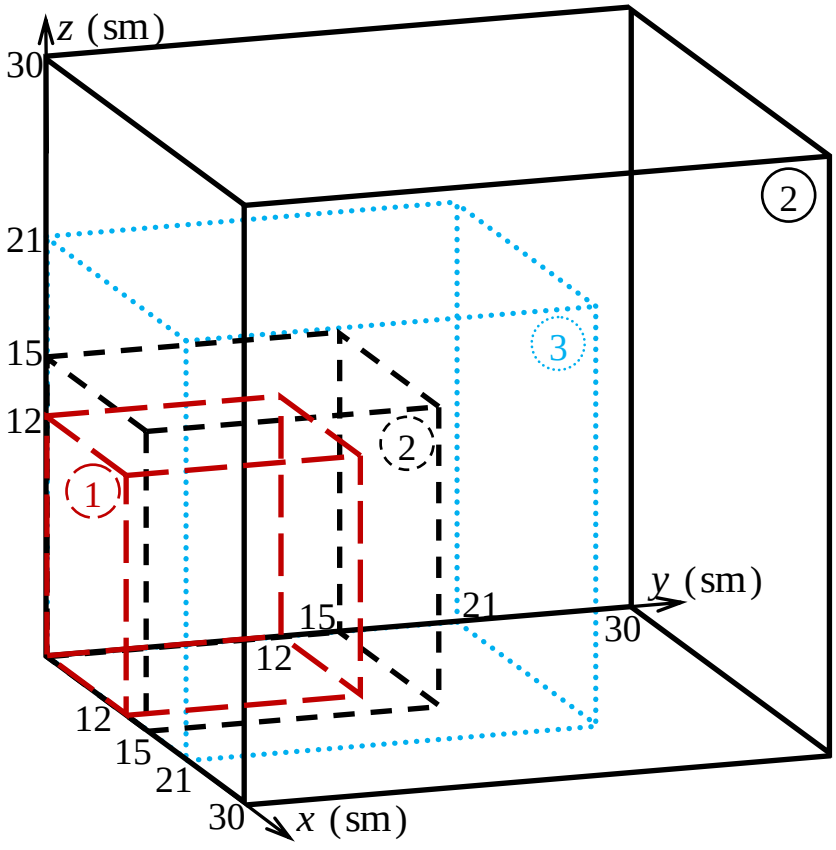

Figure 4

Geometry for the Iron-Water problem

C The Dog Leg problem [26] is a well-known benchmark problem with void region where a dog leg void is ducted through an adsorbing uniform prism. Reflective

boundary conditions with $A=1$ are used at the boundary planes $x=0$, $y=0$, and $z=0$, and vacuum (non-reflective with $\mathbf{q}_d^{\partial V}=\mathbf{0}$) boundary conditions at all other outer boundaries. The problem is solved on the S_{12} [27] angular quadrature set and on the unstructured tetrahedral spatial mesh of the 8990 cells and the 18959 faces with the nine various settings of the total and scattering cross-sections in the adsorbing material **3**. Materials properties and geometry for this problem are presented in the *Table 3* and the *Figure 5*.

Table 3

Materials properties for the Dog Leg problem

Material	**1**	**2**	**3**
σ_t (cm^{-1})	As in **3**	0.001	As per setting
σ (cm^{-1})		0.0005	
Source (cm^{-3})	1.0	0.0	0.0

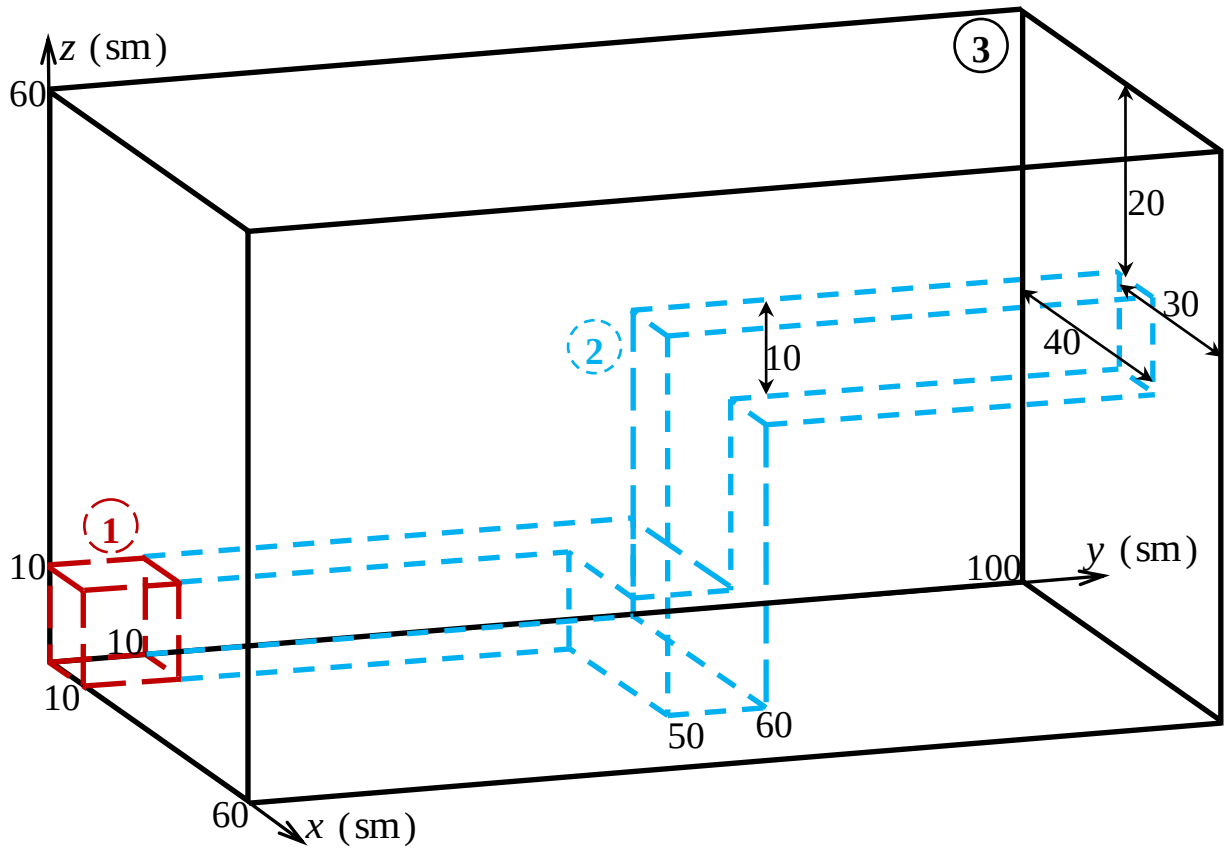

Figure 5

Geometry for the Dog Leg problem

Features of the sequentially with fineness increase enumerated meshes for the test problems A and B and the decimally enumerated settings for the test problem C are listed below along with numerical results.

Numerical results

The model test problems angular discretizations are spatially approximated on the unstructured tetrahedral meshes by the two nodal schemes [21] “ThetraC” or “ThetraL” and numerically solved by the plain source iteration (SI) method or the above produced KP_1 method. To estimate the KP_1 method efficiency in comparison to the source iterations method for the both numerical iterative methods their run times for convergence are measured for the each statement of the each problem. The KP_1 method “P_1” steps summarized calculating time are measured to estimate immediately the P_1 synthetic acceleration efficiency.

Table 4

Numerical results for the EIR-2a problem

Mesh	Amount of						SI and KP_1 run times ratio		P_1 calculating time percentage	
	Cells	Faces	Iterations							
			ThetraC		ThetraL		ThetraC	ThetraL	ThetraC	ThetraL
			SI	KP_1	SI	KP_1				
1	576	1232	275	5	278	5	4.5	24.6	0.47‰	0.33‰
2	1059	2342	279	6	281	4	22	31	0.6‰	0.5‰
3	3276	6851	309	5	317	5	11.5	30.2	9.10%	10%
4	6912	14144	361	8	372	7	9.1	26.1	15.40%	9.30%
5	12708	26312	374	6	395	5	10.9	32.7	10.60%	9.10%
6	24206	50603	350	6	365	6	9.4	24.6	13.40%	11.40%

Table 5

Numerical results for the Iron-Water problem

Mesh	Amount of						SI and KP_1 run times ratio		P_1 calculating time percentage	
	Cells	Faces	Iterations							
			ThetraC		ThetraL		ThetraC	ThetraL	ThetraC	ThetraL
			SI	KP_1	SI	KP_1				
1	384	832	745	7	753	7	63	49.5	1‰	0.7‰
2	1622	3495	764	6	774	7	35.3	52.9	15%	1.1‰
3	4608	9472	909	10	931	11	16.7	37.8	25%	17%
4	6299	13104	816	7	832	8	14.1	31.4	33%	19%
5	13854	28713	882	8	907	9	9.4	25.3	46%	35%
6	18295	38142	925	7	962	8	11.7	32	35%	27%
7	26787	55254	961	8	1002	9	9.6	25.7	42%	34%

Table 6
Numerical results for the Dog Leg problem

Setting	**Material 3**			Amount of iterations				SI and KP_1 run times ratio		P_1 calculating time percentage	
	σ_t (cm^{-1})	σ/σ_t	σ (cm^{-1})	ThetraC		ThetraL		ThetraC	ThetraL	ThetraC	ThetraL
				SI	KP_1	SI	KP_1				
1.1	0.5	0.9	0.45	128	14	139	15	1.8	4.1	35%	22%
1.2	0.5	0.95	0.475	197	13	209	16	2.6	5.4	42%	20%
1.3	0.5	0.99	0.495	431	14	456	17	3.9	9	43%	33%
2.1	1	0.9	0.9	175	16	188	19	2.3	4.7	16%	11%
2.2	1	0.95	0.95	268	14	282	18	3.5	7.1	23%	16%
2.3	1	0.99	0.99	616	15	639	18	5.6	12.7	59%	29%
3.1	1.5	0.9	1.36	215	17	228	20	2.9	5.7	24%	16%
3.2	1.5	0.95	1.425	318	16	330	19	4	8.2	31%	19%
3.3	1.5	0.99	1.485	734	16	752	18	7.1	15.8	49%	34%

For the each model test problem and the each spatial discretization scheme numbers of iterations for convergence of the both numerical iterative methods, ratios of the SI and KP_1 run times, and percentages of the "P_1" steps in the KP_1 method calculations time are listed in the *Table 4*, *Table 5*, and *Table 6* above.

Numerical solving of the "P_1" step equations is performed by the open realization [24] of the preconditioned [23] generalized minimal residual [22] Krylov method with the tolerance 10^{-8} and the Krylov subspace dimensionality equals to 5 for the test problems A and B. The same tolerance and Krylov subspace of a size 20 are used for the test problem C. This increases memory usage as compared to the 5 vectors subspace but does considerably affect the neither KP_1 method nor immediately P_1 synthetic acceleration efficiencies.

The number of iterations for convergence of the plain source iterations (SI) method increases along with the fineness of the spatial mesh for the test problems A and B, or with the total cross-section σ_t and the ratio σ/σ_t of the scattering and total cross-sections for the test problem C. On the contrary, the number of iterations for convergence of the KP_1 method remains rather persistent with the statements and spatial difference schemes change for the each test problem. That indicates that the P_1 synthetic acceleration at the each KP_1 iteration provides quite a good approximation of the additive correction for its "K" step.

Due to order lowering of the polynomial spatial approximation in the procedure of the consistent synthetic "P_1" step equations production, the SI and KP_1 run times (speeding-up) ratios of the ThetraL scheme calculations multiply greater than the

ThetraC ones. In the KP_1 method calculations the "P_1" steps summarized time could come to a slightly more than half of a full calculation run time.

The run time speeding-up of the both spatial schemes calculations increases along with the number of iterations for convergence of the source iterations (SI) method. The Iron-Water problem number of iterations for convergence of the SI method is the greatest one along with the calculation run time speeding-up for this problem. The run time speeding-up of the both spatial schemes calculations decreases along with rise of the number of iterations for convergence of the KP_1 method. Due to high anisotropy of the Dog Leg problem solution and the additive correction angular approximation linearity in the "P_1" step, for this problem the number of iterations for convergence of the KP_1 method and the calculation run time speeding-up are is the greatest and the least ones respectively.

The listed in the *Table 7* mean run time speeding-ups of the both nodal schemes calculations for each model problem are rather high.

Table 7

Test problems mean run time speeding-up

Problem		EIR-2	Iron-Water	Dog Leg
Run time speeding-up	ThetraC	10	15	4
	ThetraL	28	35	8

The relative scalar flux increment is

$$\mathrm{E} = \max_{j^{\mathrm{th}}\,\mathrm{mesh\,cell}} \left| 1 - \left(\sum_d w_d \overset{\iota+1}{\psi}_{jd} \right) \Big/ \left(\sum_d w_d \overset{\iota}{\psi}_{jd} \right) \right|, \qquad (51)$$

where

$\overset{\iota}{\psi}_{jd}$ – the value in the mesh cell j of the within-group flux distribution along the angular direction $\mathbf{\Omega}_d$ resulted from the SI or KP_1 iteration number ι.

The relative scalar flux increment (51) values dependencies on iteration number ι of the SI or KP_1 methods is plotted below for the each spatial discretization of the most difficult calculation statements of the each model test problem.

The SI convergence oscillatory for the ThetraL scheme spatial approximation of the EIR-2, Iron-Water, and Dog Leg problems is depicted in the *Figure 7*, *Figure 9*, and *Figure 11* respectively. The *Figure 6* and *Figure 7*, *Figure 8* and *Figure 9* depict the KP_1 convergence non-oscillatory for the ThetraC and ThetraL spatial difference schemes of the EIR-2 and Iron-Water problems respectively. On the contrary, the KP_1 convergence oscillatory for both spatial difference schemes of the Dog Leg problem is depicted in the *Figure 10* and *Figure 11*. That behavior may be explained by the insufficiency of the linear angular approximation of the additive correction in the "P_1" step due to the high anisotropy of the Dog Leg problem solution.

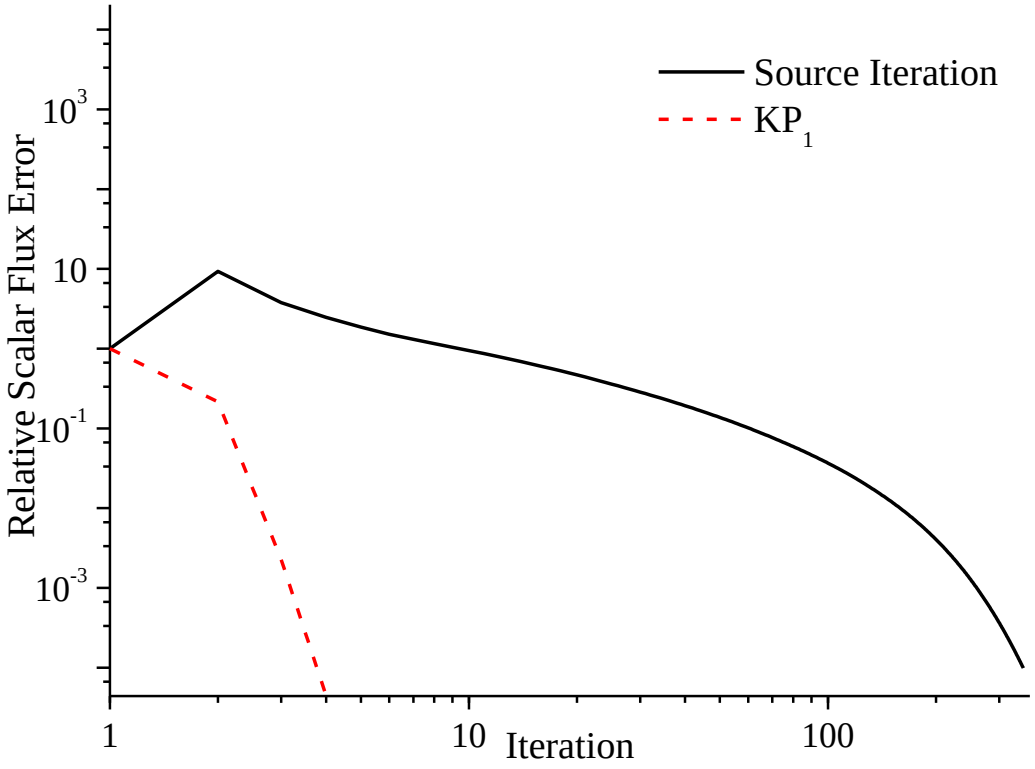

Figure 6

Relative scalar flux increment for the EIR-2a problem S_8 ThetraC source iterations (SI) and KP_1 calculations on the spatial mesh 6

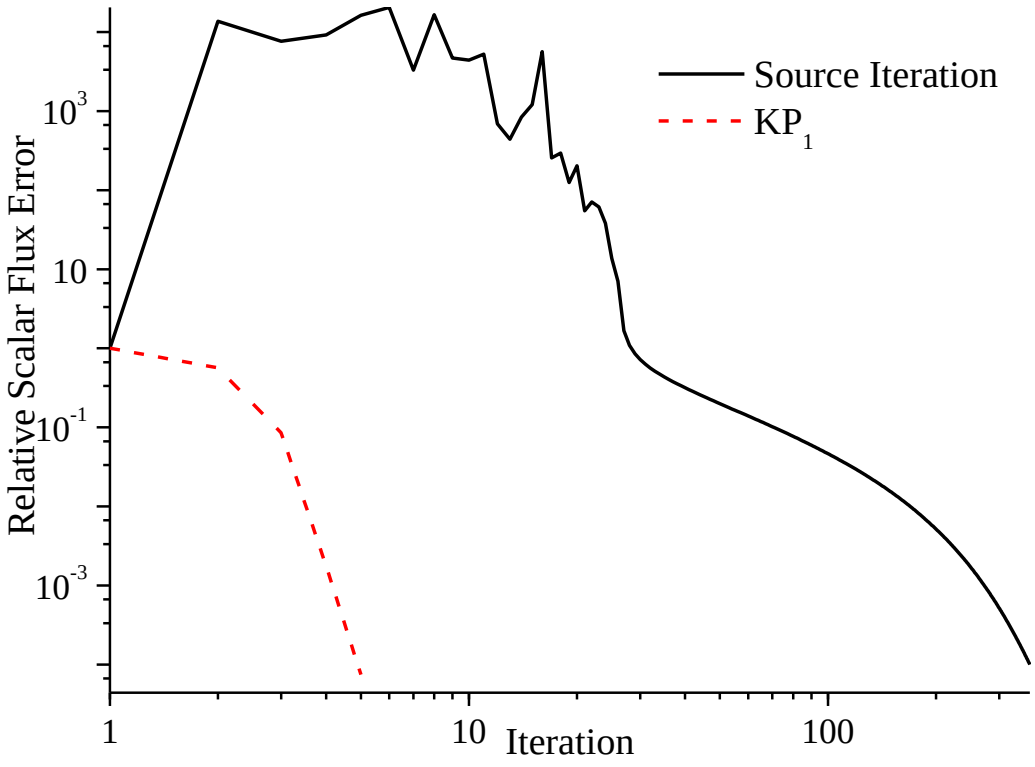

Figure 7

Relative scalar flux increment for the EIR-2a problem S_8 ThetraL source iterations (SI) and KP_1 calculations on the spatial mesh 6

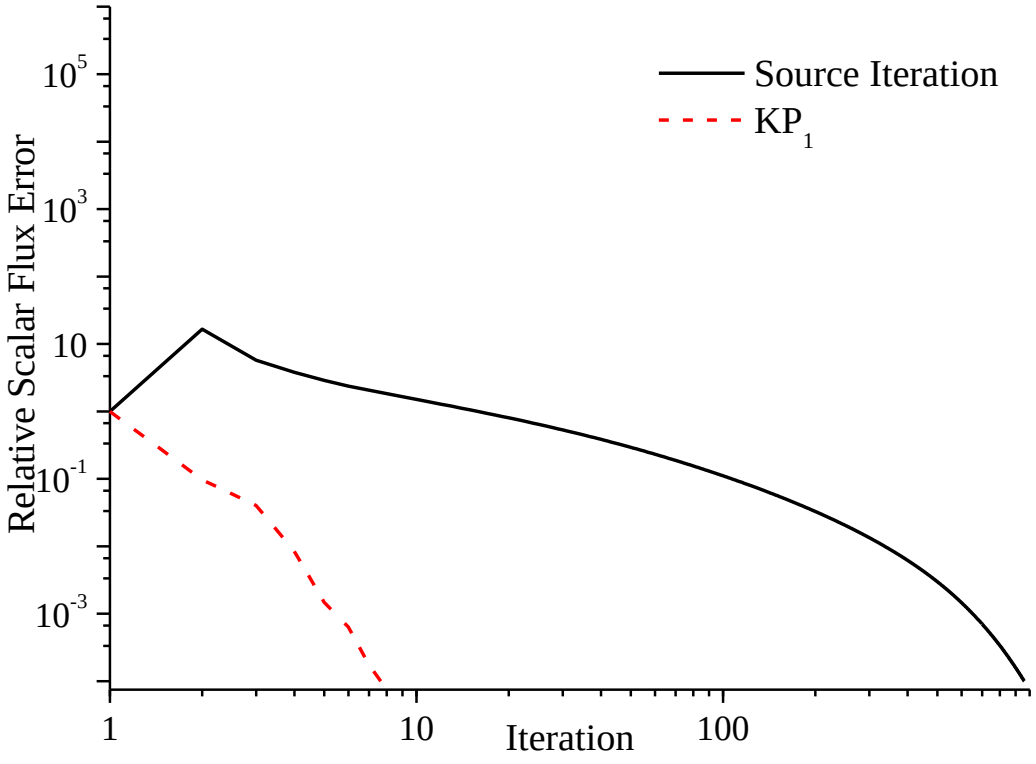

Figure 8

Relative scalar flux increment for the Iron-Water problem S_8 ThetraC source iterations (SI) and KP_1 calculations on the spatial mesh 7

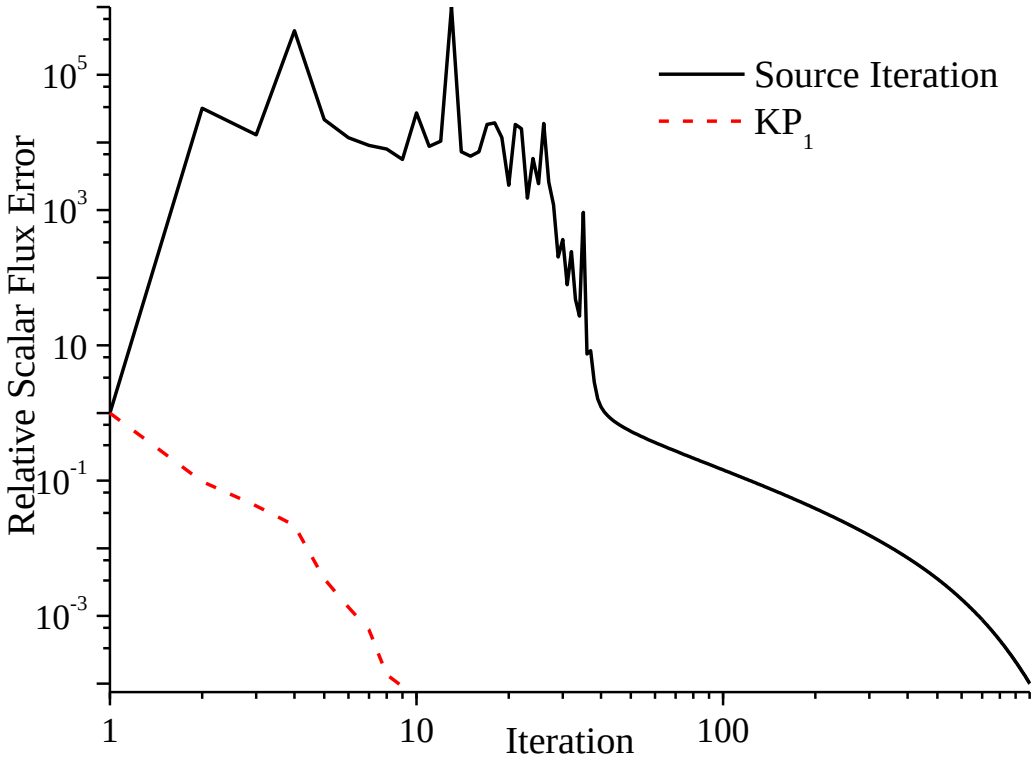

Figure 9

Relative scalar flux increment for the Iron-Water problem S_8 ThetraL source iterations (SI) and KP_1 calculations on the spatial mesh 7

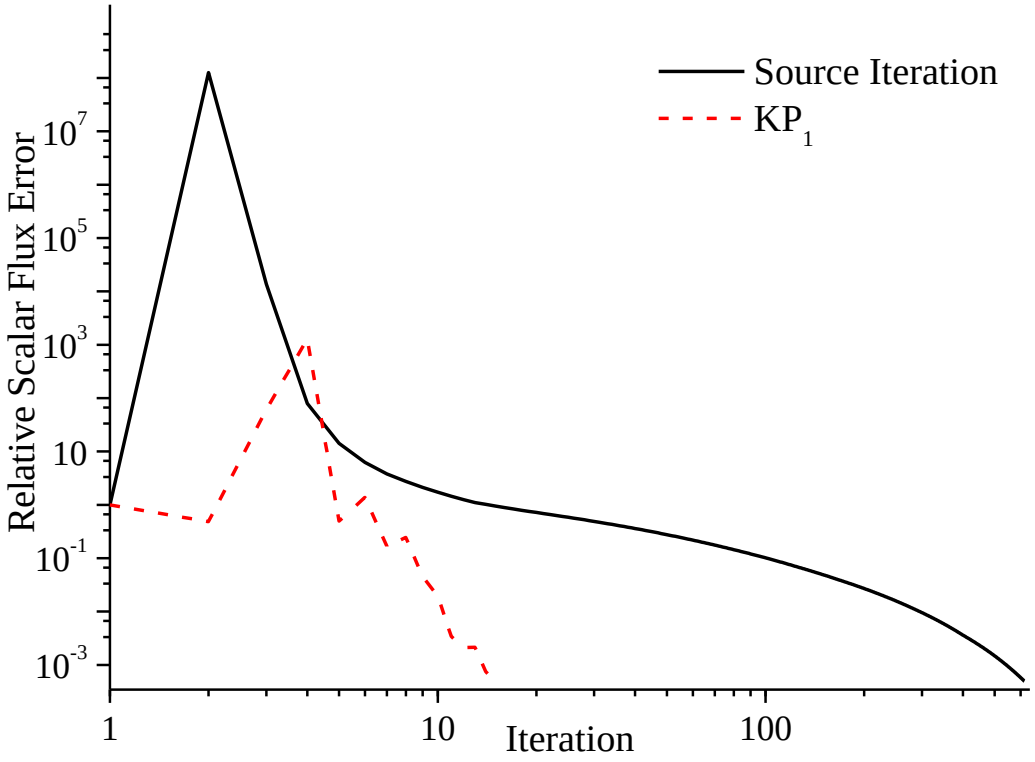

Figure 10

Relative scalar flux increment for the Dog Leg problem S_{12} ThetraC source iterations (SI) and KP_1 calculations with setting 2.3

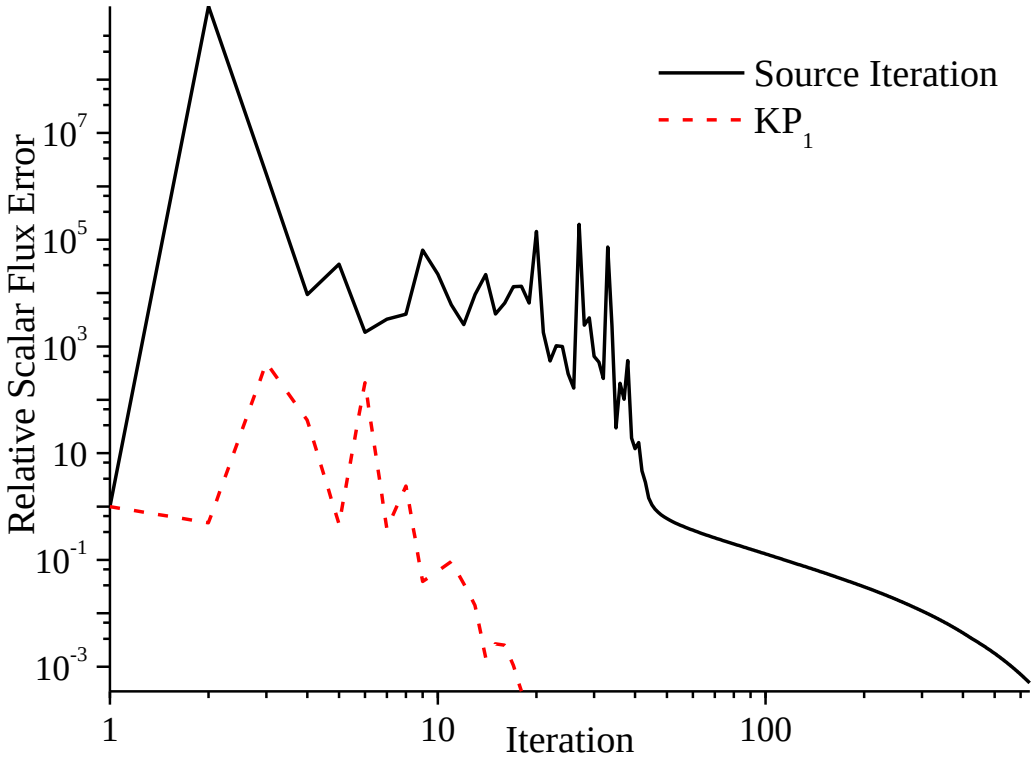

Figure 11

Relative scalar flux increment for the Dog Leg problem S_{12} ThetraL source iterations (SI) and KP_1 calculations with setting 2.3

Conclusions

For the iterative KP method the production procedure of the consistent low-order P_1 synthetic equations system in the additive correction is presented. This system may be applied to accelerate the inner transport iterations in 3D geometry. The derivation is based on the linear in solid angle approximation of the additive correction and requirement of the spatial approximations consistency of the base within-group S_N transport equation and the resulting synthetic ones. The latter condition is necessary for the resulting KP_1 method solution convergence to the solution of the within-group S_N transport equation.

To obtain the KP_1 nodal transport calculations algorithm, the constant nodal schemes for the S_N transport equation spatial approximation is numerically integrated over solid angle. Usage of the only constant schemes leads to the spatial order lowering of the produced P_1 synthetic equations consistent spatial approximation. In the algorithm at the each iteration of the KP_1 method the low-order P_1 synthetic equations system in the additive correction linear angular approximation coefficients is produced by the base equation spatial approximation integration over solid angle and solved by the preconditioned generalized minimal residual Krylov method.

The developed algorithm is tested on the three well-known model heterogeneous one-group neutron transport problems. The 3D modifications of the problems were previously triangulated, thus base model transport problems are approximated on several unstructured tetrahedral meshes by the two nodal schemes. Performances on the model test problems of the developed iterative KP_1 method algorithm and the plain source iteration (SI) method algorithm are compared to each other.

The KP_1 nodal calculations demonstrate oscillatory for the problem with highly anisotropic solution but high efficiency of the nodal transport iterations acceleration on all problems. The worst performance acceleration is demonstrated on the Dog Leg benchmark problem with void region. The best performance acceleration is demonstrated on the Iron-Water problem that simulates PWR.

Reference

1. G. I. Bell, S. Glasstone "Nuclear Reactor Theory" Van Nostrand Reinhold Co., New York, 1970.
2. M. L. Adams, E. W. Larsen "Fast iterative methods for discrete-ordinates particle transport calculations" Progress in Nuclear Energy, Volume 40, Issue 1, 2002, Pages 3-159. DOI:10.1016/S0149-1970(01)00023-3
3. V. Y. Goldin "A quasi-diffusion method of solving the kinetic equation" USSR Computational Mathematics and Mathematical Physics, Volume 4, Issue 6, 1964, Pages 136-149. DOI:10.1016/0041-5553(64)90085-0
4. D. Y. Anistratov, V. Y. Goldin "Nonlinear methods for solving particle transport problems" Transport Theory and Statistical Physics, Volume 22, Issue 2-3, 1993, Pages 125-163. DOI:10.1080/00411459308203810
5. E. N. Aristova, D. F. Baydin "Efficiency of quasi-diffusion method for calculating critical parameters of a fast reactor" Mathematical Models and Computer Simulations, Volume 4, Issue 6, 2012, Pages 568-573. DOI:10.1134/S2070048212060026
6. E. N. Aristova, D. F. Baydin "Implementation of the quasi-diffusion method for calculating the critical parameters of a fast neutron reactor in 3D hexagonal geometry" Mathematical Models and Computer Simulations, Volume 5, Issue 2, 2013, Pages 145-155. DOI:10.1134/S2070048213020026
7. T. A. Germogenova, T. A. Sushkevich "An average fluxes method of solving the transport equation" Problems of Reactor Shielding Physics, Number 3, Atomizdat, 1969, Pages 34-46. (in russian)
8. A. M. Voloschenko, T. A. Germogenova "Numerical solution of the time-dependent transport equation with pulsed sources" Transport Theory and Statistical Physics, Volume 23, Issue 6, 1994, Pages 845-869. DOI:10.1080/00411459408203929
9. V. I. Lebedev "An iterative KP-method" USSR Computational Mathematics and Mathematical Physics, Volume 7, Issue 6, 1967, Pages 53-78. DOI:10.1016/0041-5553(64)90085-0
10. A. M. Voloshchenko "KP_1 acceleration scheme for inner iterations consistent with the weighted diamond differencing scheme for the transport equation in three-dimensional geometry" Computational Mathematics and Mathematical Physics, Volume 49, Issue 2, 2009, Pages 334-362. DOI:10.1134/S0965542509020134
11. H. J. Kopp "Synthetic method solution of the transport equation" Nuclear Science and Engineering, Volume 17, Number 1, 1963, Pages 65-74. DOI:10.13182/NSE63-1
12. R. E. Alcouffe "Diffusion synthetic acceleration methods for the diamond-differenced discrete-ordinates equations" Nuclear Science and Engineering, Volume 64, Number 2, 1977, Pages 344-355. DOI:10.13182/NSE77-1

13. J. E. Morel "Synthetic acceleration method for discrete ordinates calculations with highly anisotropic scattering" Nuclear Science and Engineering, Volume 82, Number 1, Pages 34-46.
14. E. W. Larsen "Unconditionally stable diffusion-synthetic acceleration methods for the slab geometry discrete ordinates equations. Part I: Theory" Nuclear Science and Engineering, Volume 82, Number 1, 1982, Pages 47-63. DOI:10.13182/NSE82-1
15. D. R. McCoy, E. W. Larsen "Unconditionally stable diffusion-synthetic acceleration methods for the slab geometry discrete ordinates equations. Part II: Numerical results" Nuclear Science and Engineering, Volume 82, Number 1, 1982, Pages 64-70. DOI:10.13182/NSE82-2
16. E. W. Larsen "Diffusion-synthetic acceleration methods for discrete-ordinates problems" Transport Theory and Statistical Physics, Volume 13, Issue 1-2, 1984, Pages 107-126. DOI:10.1080/00411458408211656
17. H. Khalil "A nodal diffusion technique for synthetic acceleration of nodal S_N calculations" Nuclear Science and Engineering, Volume 90, Number 3, 1985, Pages 263-280.
18. B. Turcksin, J. C. Ragusa "Discontinuous diffusion synthetic acceleration for transport on 2D arbitrary polygonal meshes" Journal of Computational Physics, Volume 274, 2014, Pages 356-369. DOI:10.1016/j.jcp.2014.05.044
19. I. R. Suslov "An algebraic collapsing acceleration method for acceleration of the inner (scattering) iterations in long characteristics transport theory" International Conference on Supercomputing in Nuclear Applications, Paris, France, September 22-24, 2003.
20. R. Le Tellier, A. Hébert "An improved algebraic collapsing acceleration with general boundary conditions for the characteristics method" Nuclear Science and Engineering, Volume 156, Number 2, 2007, Pages 121-138.
21. O. V. Nikolaeva "Nodal scheme to the radiation transport equation on unstructured tetrahedral mesh" Mathematical Models and Computer Simulations, 2015. (in print)
22. Y. Saad, M. H. Schultz "GMRES: A generalized minimal residual algorithm for solving nonsymmetric linear systems" SIAM Journal on Scientific and Statistical Computing, Volume 7, Issue 3, 1986, Pages 856-869. DOI:10.1137/0907058
23. Y. Saad "A flexible inner-outer preconditioned GMRES algorithm" SIAM Journal on Scientific Computing, Volume 14, Issue 2, 1993, Pages 461-469. DOI:10.1137/0914028
24. N. I. Kokonkov "GMRES(m) algorithms implementation", KIAM (RAS), 2012. http://cpt.imamod.ru/alg/krylov/cpt-2012_geminres.pdf
25. A. Kavenoky, J. Stepanek, F. Schmidt "Benchmark problems" Transport theory and advanced reactor calculations, IAEA-TECDOC-254, International Atomic Energy Agency, October 1981, Pages 305-323.

26. K. Kobayashi, N. Sugimura, Y. Nagaya "3D radiation transport benchmark problems and results for simple geometries with void region" Progress in Nuclear Energy, Volume 39, Issue 2, 2001, Pages 119-144. DOI:10.1016/S0149-1970(01)00007-5
27. B. G. Carlson, C. E. Lee "Mechanical quadrature and the transport equation" Los Alamos Scientific Laboratory Report, LAMS-2573, June 1961.